Int J Appl Earth Obs Geoinformation 80 (2019) 71–81

Contents lists available at ScienceDirect

Int J Appl Earth Obs Geoinformation

journal homepage: www.elsevier.com/locate/jag

# Arctic climate and snow cover trends – Comparing Global Circulation Models with remote sensing observations

Darri Eythorsson[a,*], Sigurdur M. Gardarsson[a], Shahryar K. Ahmad[b], Faisal Hossain[b], Bart Nijssen[b]

[a] Faculty of Civil and Environmental Engineering, University of Iceland, Iceland
[b] Faculty of Civil and Environmental Engineering, University of Washington, United States

ARTICLE INFO

*Keywords:*
Snow Cover Frequency
Köppen-Geiger climate classifications
MODIS
Google Earth Engine
Trend analysis

ABSTRACT

This study assessed the impact of climate change on snow resources in the Arctic. Climate was classified for the period 1950–2100 according to the Köppen-Geiger (KG) classification system using the ensemble average of NASA-NEX CMIP5 projections for the rcp 4.5 scenario. Snow Cover Frequency (SCF) in days/year was calculated from the MODIS10A1 snow product and the SCF trends were calculated across the Arctic for the MODIS period (2001–2016). Ten pollution monitoring areas in the Arctic lowlands, especially vulnerable to climate change impacts, were selected for analyzing the climate and snow regimes. In seven of the ten areas we observed significant changes in the climate during the MODIS period and these same areas also showed the largest SCF trends. At lower latitudes we observed decreasing SCF, while further north, by the shores of the Arctic seas, SCF has increased. Averaged across the Arctic we observed a 0.91 days/year decrease in SCF. Our results show that across the Arctic warmer climate classes have and will continue to replace polar tundra and cold summer regions. Based on the CMIP5 simulations, we expect the coverage of the currently dominant Arctic climate class, Cold climate with cold summers and no dry season (*Dfc),* to decline by about 40% by 2100 and be replaced by climate classes associated with warm (*Dfb, Dsb, Dwb*) and hot (*Dfa, Dsa, Dwa*) summers.

## 1. Introduction

We studied the impact of climate change on snow resources in the Arctic. The historical and future expected climate warming was assessed, as estimated by Global Circulations Model (GCM) projections for the rcp 4.5 scenario. We combined information on the climate trends with satellite observations of snow cover to investigate the climate impact on snow resources in the area. The results were analyzed to identify physical drivers for the observed changes on a regional basis and assess the future evolution of the Arctic snow regime. The specific research questions we considered were whether there has been and/or can we expect significant changes in the Arctic climate and, if climate change has occurred, can it be detected by remote sensing observations of the local snow cover?

The climate in the Arctic has been warming at twice the global rate and polar regions are expected to experience the most rapid climate change globally (Larsen et al., 2015). Among the impacts that have been observed already are melting permafrost (Lawrence et al., 2008), declining sea ice concentrations (Notz and Stroeve, 2016), species migrations (Thuiller et al., 2008) and extreme weather events (Cohen et al., 2014). These impacts, which are expected to further advance in the future, will drastically impact Arctic societies and ecosystems (Overland et al., 2013). An essential factor for societal adaptation in the Arctic will be to understand the impact of changing climate regimes on local water resources, which are stored in the landscape as ice and snow for large portions of the year (Diffenbaugh et al., 2013; Eliasson et al., 2017).

A key estimate of the availability of snow resources from remote sensing is Snow Cover Frequency (SCF), the number of snow-covered days per year. SCF can indicate growing season length and habitat suitability (Barichivich et al., 2013) and is an important geophysical feature as snow cover will reflect most of the inbound solar radiation (Cohen, 1994). As it is an important element in several land surface processes, SCF is an important variable in geophysical simulations, e.g. hydrological modelling in cold regions (Bokhorst et al., 2016). Due to its importance, snow cover has been a key observation target for remote sensing using satellites since the 1960's (Cohen, 1994; Guan et al., 2013). Many instruments have been deployed to map global snow cover using various sensor technologies including optical sensors (e.g. Landsat, AVHRR, MODIS, GOES) and microwave technology (e.g. SMMR and AMSR-E) (Dietz et al., 2012). Data from these sensors have, for example, been assimilated in hydrological models to improve

* Corresponding author.
*E-mail address:* dae5@hi.is (D. Eythorsson).

https://doi.org/10.1016/j.jag.2019.04.003
Received 26 November 2018; Received in revised form 3 April 2019; Accepted 8 April 2019
Available online 16 April 2019
0303-2434/ © 2019 Elsevier B.V. All rights reserved.

streamflow simulations (Huang et al., 2017).

Among the best estimates of future climate conditions are GCM projections, whose skill has improved in recent years and which are the basis for developing and implementing societal adaptation strategies (Stocker et al., 2013). We used the ensemble average of the CMIP5 projections for the Representative Concentration Pathway (rcp) 4.5 emission scenario to represent historical and future climate conditions, respectively (Taylor et al., 2012). The GCM output can be used to classify regional climate into different climate regimes. Climate change can then be quantified by analyzing changes of these regimes over time (Chen and Chen, 2013). A widely accepted classification scheme is the Köppen-Geiger (KG) climate classification system, which classifies climate regimes based on temperature and precipitation estimates (Köppen, 1918). The KG system has been used in a variety of disciplines to estimate both global and local impacts of climate change (Chen and Chen, 2013) and as a method to validate GCM results (Lohmann et al., 1993). With the availability of gridded high resolution climate simulations and improved computational capabilities, these maps can now be produced with higher spatial and temporal resolution allowing for a more detailed analysis of climate changes (Kottek et al., 2006; Spinoni et al., 2015).

In this study we analyzed SCF trends using MODIS data that is available for the period (2001–2016) to investigate how they compare with climate changes predicted by recent GCM projections. We argue that if significant changes in the climate and snow regimes coincide in space and time, longer term GCM projections can be considered more reliable and can be used to predict long term SCF trends.

Our hypothesis is that the warming trend that has been observed in the Arctic would result in a decreasing trend in snow cover across the area. We expect this trend to be more pronounced at lower latitudes but also present further north. Our results indicate that the interaction between the climate and snow regimes is not this straightforward, as in some locations we observed a significant increase in SCF simultaneously with a shift toward warmer climate.

## 2. Materials and methods

### 2.1. Tools and datasets

In this study the Google Earth Engine (GEE) (Gorelick et al., 2016) was used for all spatial analysis, while some of the statistical analysis and plotting of the results was performed in Python using the SciPy toolbox (Oliphant, 2007). All the datasets used in the study were available in the GEE data catalog. Graphs were created using Pyplot and maps were produced in ArcGIS.

Representative Concentration Pathway (rcp) 4.5 is a stabilization scenario in which total radiative forcing will be stabilized before 2100 by employment of a range of technologies and strategies for reducing greenhouse gas emissions (van Vuuren et al., 2011). The NASA NEX dataset (Thrasher et al., 2006) was used to estimate daily climate conditions by calculating the ensemble average of the CMIP5 projections for the rcp 4.5 scenario (van Vuuren et al., 2011; Taylor et al., 2012). The NASA NEX dataset contains downscaled projections of the 21 GCMs from the CMIP5 model inter-comparison project (Taylor et al., 2012). The CMIP5 calculations were performed in support of the fifth assessment report of the International Panel on Climate Change (IPCC AR5) (Taylor et al., 2012). The NASA NEX dataset is bias-corrected as it contains the CMIP5 GCM reproduction of historic climate.

The MOD10A1.005 MODIS/Terra dataset was used for daily snow cover classifications. The GE data catalog provides the MODIS global daily snow cover products MOD10A1 (Terra) and MYD10A1 (Aqua) (Hall et al., 2006). These datasets contain gridded daily snow cover identified using the Normalized Difference Snow Index (NDSI). The MODIS/Terra product was selected over MODIS/Aqua due to the failure of the band 6 detectors on MODIS/Aqua which impact the calculation of the NDSI (Barnes et al., 2003). Several studies conducted to validate the MODIS snow products have shown good performance compared to other satellite-derived snow results (Maurer et al., 2003) and to ground observations (Xu et al., 2017). The MOD09GA dataset from NASA EOSDIS LP DAAC was used for information about the nadir angle of the MODIS observations.

For calculations involving elevation, we used the GTOPO30 30 arc-second global digital elevation model (LP-DAAC, 2004).

### 2.2. Study areas

We selected ten pollution monitoring areas within the Arctic boundary defined by the Arctic Monitoring and Assessment Program (AMAP) of the Arctic Council as our study areas. For comparison, analysis was also performed for the entire AMAP area. These ten areas were selected as they are considered especially vulnerable to human development and climate change (AMAP, 2015). The study areas were restricted to the Arctic coastline and lowlands and code was written in GEE to select only data from elevations below 500 m a.s.l. The study areas are shown in Fig. 1. The study areas refer to 70% of the total AMAP area and 92% of the AMAP area below 500 m.a.s.l. We analyzed the Arctic lowlands in our study, because we expect the greatest changes to the climate and snow regimes in these areas. Furthermore, these lower elevation areas are where most human development is located and are the most important areas for wildlife and vegetation habitat. At higher elevation in the Arctic, where glaciation is much more common, large changes in snow or climate were not expected and any changes would be of less consequence for Arctic societies and ecology.

The study areas were manually approximated using the geography tools in the JavaScript version of GEE, while the AMAP boundary was obtained and uploaded as an asset to GEE. The AMAP boundary and the selected pixels of the study areas are shown in Fig. 1.

### 2.3. Climate classification trends

KG climate classifications were calculated globally at 0.2-degree horizontal resolution. We implemented an algorithm in GEE to classify each pixel based on the KG classification criteria which are summarized in Appendix A (Kottek et al., 2006; Peel et al., 2007). The classification consists of five main classes, each with two levels of subclasses, yielding a total of 30 climate classes. Thus, for example, an area classified with the main class *D – Cold*, second subclass *f – no dry season* and the third subclass *b – warm summer*, would have the code *Dfb*. The algorithm was applied to the Arctic region to calculate annual KG classifications for the duration of the NASA NEX dataset (1951–2100) for the rcp 4.5 scenario.

The ensemble average of the climate models was calculated and taken as an estimate of future conditions. We chose to use the ensemble average of the 21 GCMs in the NEX dataset for rcp 4.5 to run the KG categorical classification scheme. We used the ensemble average as this is a good representative of the of future climate states defined by the rcp 4.5 scenario of the CMIP5 GCM ensemble.

For this study, climate change was estimated as a change in the KG classification for each grid cell due to a change in temperature and precipitation patterns in that same grid cell over varying time periods (Beck et al., 2005). The proportional coverage of each climate class within each study area was found for each year, yielding a time series of proportional KG class coverage in each area. We calculated KG classes for the full period of the NEX dataset (1951–2099) while SCF was estimated using MODIS data available for the period (2001–2016). We

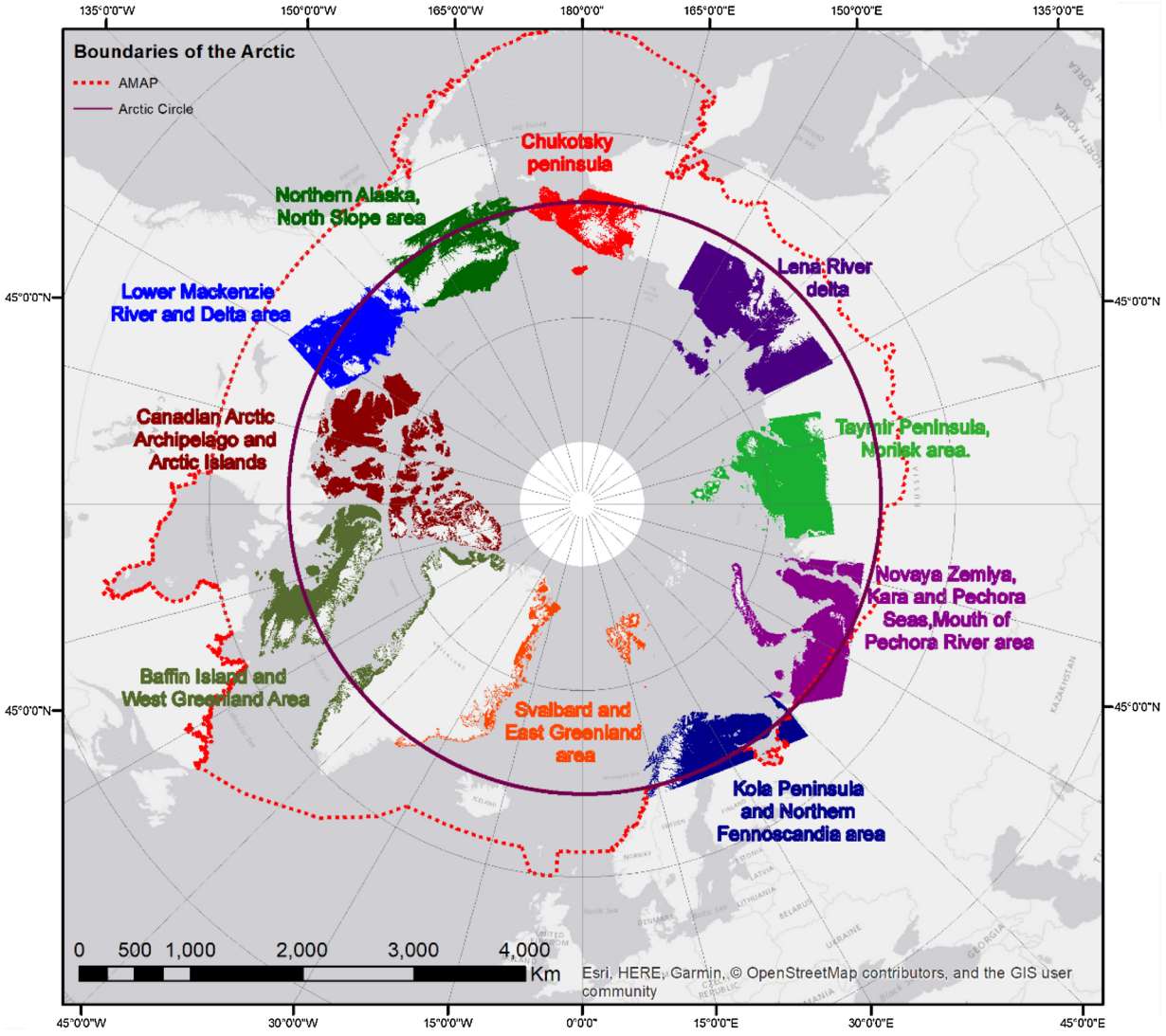


**Fig. 1.** The Arctic AMAP area and the selected pixels of the ten study areas below 500 m. a.s.l.
Data: AMAP (2015).

used the SCF time series to attempt to validate the GCM projections as we argue that significant changes in the climate and snow regime should coincide in time and space; the projections can then be used to predict future SCF trends and to assess them for periodicity.

### 2.4. Snow cover frequency trends

We calculated annual SCF at a 500 m × 500 m resolution across the Arctic based on the MODIS10A1.005 snow cover product. We re-mapped the MODIS10A1 dataset to provide a binary classification of snow cover for all valid observations by assigning pixels with value 1 (snow/ice) or 0 (no snow/ice). Observations with zenith angles greater than 25° were filtered out to reduce the so-called *panoramic "bow-tie" effect*. This is a panoramic distortion that is exacerbated by the curvature of the earth, causing overlap in satellite scan lines, leading to data repetition, which is known to cause systematic error in snow mapping in general (Souri and Azizi, 2013) and decreasing accuracy of the MODIS cloud cover mask specifically (Ackerman et al., 2008). Information about the sensor nadir angle was extracted from the MOD09GA dataset and merged with the remapped MOD10A1. The snow cover detection algorithm used to develop MOD10A1 uses all the MODIS swaths acquired in a given day to select the best observation using the NDSI (Baker, 2011).

The MODIS cloud detection algorithm has been evaluated over polar areas and has exhibited misclassification rates for daytime observations of as high as 20% (Liu et al., 2004). With the release of the fifth collection of MODIS imagery significant improvements have been made to the cloud mask (Frey et al., 2008). Wang et al. (2016) compared the MODIS cloud mask to the CloudSat-Cloud-Aerosol and Infrared Pathfinder Satellite Observations (CALIPSO) (C-C) and found 77.8% agreement between the methods (Wang et al., 2016). Ackerman et al., 2008 compared the MODIS cloud mask with ground-based Lidar and satellite-borne Laser Altimeter data and found 85% agreement among the methods. Ault et al. (2006) compared the MODIS cloud cover detection to field observations and found agreement between 86–92%. Based on these studies, we used the MOD10A1 data as is, without additional cloud masking. In this study, missing observations because of, for example, cloud cover or polar night were masked by assigning them a null

value. Pixels with null values that also occurred between consecutive swaths with high nadir angles were rejected. These procedures reduced the number of valid observations annually so that across the Arctic we observed on average 60 valid observations/year per pixel

We calculated the annual SCF for each pixel by filtering the image collection by year and counting the number of times each pixel was covered in snow, dividing by the number of valid observations in each year. Annual SCF maps were calculated for the period of MODIS observations (2001–2016) based on all valid MODIS observations. We did not perform any gap-filling on the MODIS snow cover product to avoid introducing bias in case the number of valid observations is correlated to snow cover. The trend in SCF over the MODIS time series was estimated by linear regression and Sen's estimator of slope method (Sen, 1968) at each pixel. The statistical significance of the trend line was then assessed, using both the non-parametric Mann-Kendall trend test (Maurice and Kendall, 1975) and Sen's estimator of slope methods, as described in the following sections.

### 2.5. Comparing trends in KG class coverage and SCF

In each study area the timeseries of proportional KG coverage were investigated for evidence of statistically meaningful change during the period of overlap (2001–2016) using the non-parametric Mann-Kendall and Sen's estimator of slope methods. Confidence levels of $\alpha = 0.05$ and $\alpha = 0.01$ were selected as thresholds for reporting statistically significant results. The threshold values of $\alpha$ were selected as this has been a tradition in quantitative research. However, as a value of slightly less than 0.05 only provides a weak argument against the null hypothesis (Wasserstein and Lazar, 2016), p-values are reported for all analyses performed in this study to report the strength of the evidence against the null hypothesis.

The evidence for statistical significance of the trends in SCF and KG class coverage was assessed. Since the distribution of the data is unknown and not assumed to be normally distributed, we estimated the significance of trend using the non-parametric Sen's slope method (Sen, 1968) and the Mann-Kendall hypothesis test (Kendall 1975). Both of these methods have frequently been used to quantify significance of trend in hydro-meteorological time series (Drapela and Drapelova, 2011; Gocic and Trajkovic, 2013). The null hypothesis was that there was no monotonic trend in the data: $H_0$: $s = 0$, while the alternative hypothesis was that a monotonic trend was present: $H_1$: $|s| > 0$. Maps were developed showing areas with significant evidence for the rejection of the null hypothesis.

The significance of the trend identified by linear regression was assessed using the Mann-Kendall test. The test was applied using the *ee.Reducer.kendallsCorrelation()* function in GEE and the *stats.kendalltau*() function in SciPy was used. Significant values of $\tau$ were estimated from the large sample approximation which is valid for $n > 10$. *Z*-values corresponding to these significance levels were found for the standard normal distribution (Helsel and Hirsch, 2002).

The trend was also estimated using Sen's slope method, which is less sensitive to outliers. The method was applied using the *ee.Reducer.sensSlope()* function in GEE and the *stats.mstats.theilslopes*() function in SciPy. The slope was estimated between all data points in the time series and ordered from smallest to largest. Sen's slope estimate was calculated to give the mean of the slope estimates. The confidence intervals about the slope estimate were calculated for $\alpha = 0.01$ and $\alpha = 0.05$. The slope was determined to be statistically different from zero if the upper and lower confidence intervals shared the same sign (Gocic and Trajkovic, 2013).

## 3. Results

### 3.1. Trends in climate classifications

We classified Arctic climate annually for the period 1951–2100 as per the methods described in Section 2.3. We calculated the proportional coverage of each climate class in each study area for each year in the record. Our results showed that, across the Arctic and especially at lower latitudes, climate classes associated with warmer and longer summers have been replacing colder climates. Our results further show that these trends are expected to continue throughout the 21st century.

Fig. 2 shows the climate classifications for the years 1951 and 2099. The figure shows that cold climate with warm summers and no dry season (*Dfb)*, which historically has been the main climate class in the continental subarctic, will spread northward until at least the end of the current century, replacing climates associated with cold summers and very cold winters. Fig. 2 shows that all the main climate classes within the Arctic belong to the groups of Cold (*D*) or Polar (*E*) climate.

Table 1 shows the average coverage of the polar and cold climate classes within the Arctic AMAP boundary for the decades 1951–1960 and 2090–2099 grouped by sub category. Table 1 also shows the change in coverage of the same classes during this period. The results show that all classes associated with polar and cold climate with very cold winters are expected to decline during the period. On average, cold climate with cold summers is expected to decline, although the dry/cold summer class (*Dsc*) is expected to expand by half. All climate classes associate with warm and hot summers are expected to more than double during the present century. We note that KG class *Dfd*, cold climate with very cold winters and no dry season was not observed.

Fig. 3 shows the time series of proportional coverage for the main groups of climate classes in the Arctic AMAP area during the period 1951–2099 with a rolling 15-year average. Our results show that throughout the period cold climate classes with cold summers (*Dfc, Dsc* and *Dwc*) are the most common Arctic climates below 500 m.a.s.l. Fig. 3 shows that classes with very cold winters (*Dwd* and *Dsd*) and polar climates (*ET* and *EF*) decline steadily throughout the study period. Climate classes with warm (*Dfb, Dsb* and *Dwb*) and hot summers (*Dfa, Dsa* and *Dwa*) consistently increase in coverage throughout the period, with the rate of increase accelerating after year 2000. Our results show that in the beginning of the period the cold summer classes are rapidly replacing polar (*ET* and *EF*) and very cold winter (*Dwd* and *Dsd*) climate classes, with cold summer classes reaching a peak coverage around year 2020. In the latter part of the period classes with warm (*Dfb, Dwb* and *Dsb*) and hot summers (*Dfa, Dwa* and *Dsa*) advance further north into the Arctic, causing a net decline in the coverage of the cold summer climate classes.

Our results show that by the end of the 21st century the coverage of the most common Arctic climate class in the beginning of the period, cold climate with cold summers and no dry season (*Dfc*) will have decreased by about 40%. The second most common class, Polar tundra (*ET*) is expected to decrease by 34% during the same period. We expect that as these colder climate classes recede further north, climate classes associated with warm and hot summers will expand in coverage by 185% and 733% respectively.

### 3.2. SCF trends

We estimated the SCF trends in the Arctic using linear regression and the Sen's slope estimator method, as described in Section 2.4. The methods showed good agreement and yielded similar slope estimates. The evidence for the significance of the trends was estimated using the Sen's slope estimator test and the Mann-Kendall trend test for the Sen's slope and linear regression trends, respectively.

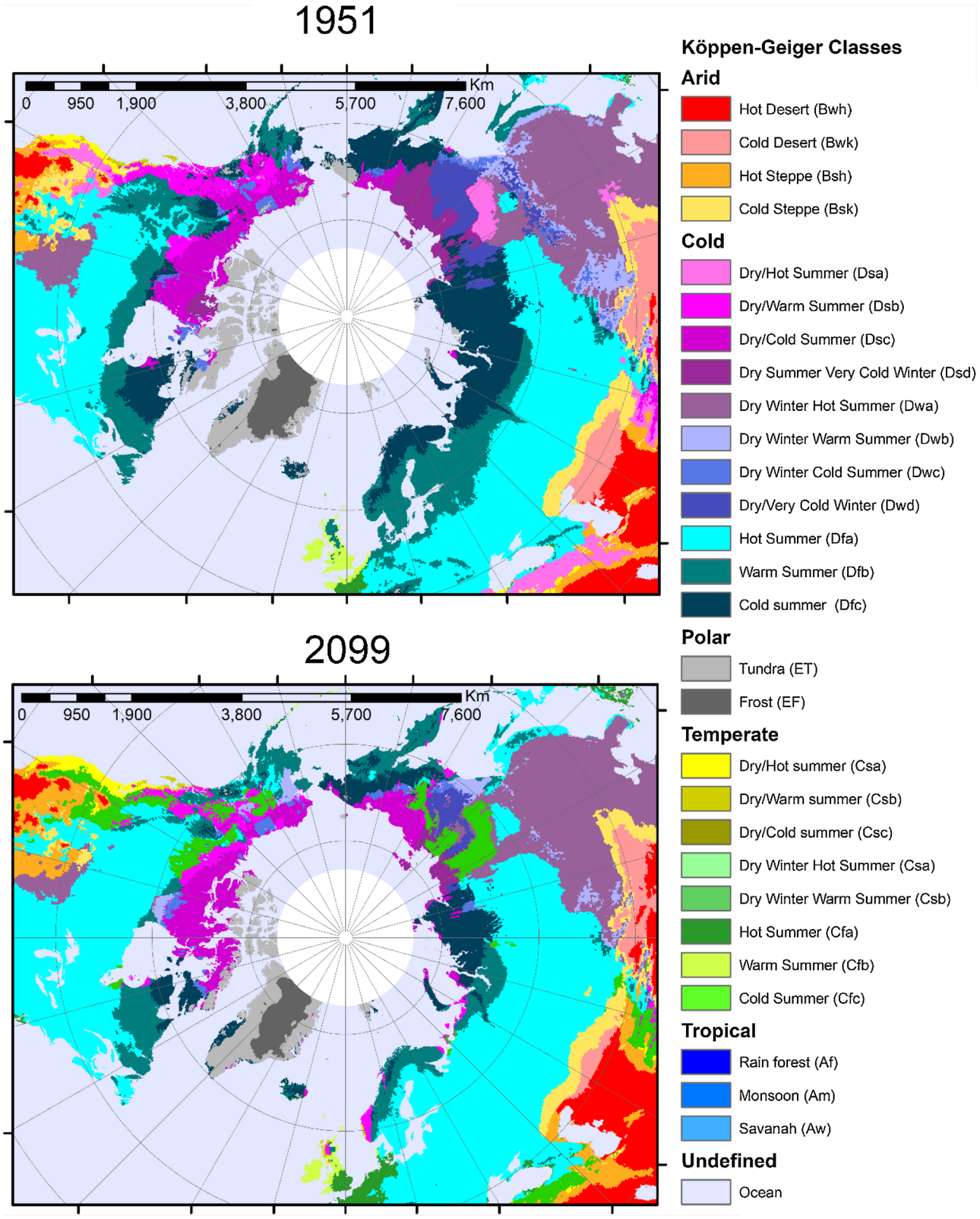


**Fig. 2.** Examples of annual Köppen-Geiger (KG) classification maps, for year 1951 (upper) and 2099 (lower).

Fig. 4 shows areas with significant SCF slope as highlighted (blue for decreasing SCF and red for increasing SCF) for both statistical methods and significance levels of $\alpha = 0.05$ and $\alpha = 0.01$. The results show that, in general, both methods identify the same areas as exhibiting significant SCF slope. However, the Mann-Kendall method identified areas with permanent snow cover as having a significant increase in SCF, most notably on the Greenland ice sheet. The Sen's method was less sensitive to outliers due to pixel misclassification and did not

**Table 1**
Coverage of Polar and Cold climate classes within the Arctic AMAP boundary and changes between 1951–1960 and 2090–2099.

| | | 1951–1960 | 2090–2099 | Net Change |
|---|---|---|---|---|
| | **Polar** | **26.4%** | **17.3%** | **−35%** |
| | Polar Frost (EF) | 0.4% | 0.1% | −86% |
| | Polar Tundra (*ET*) | 26.0% | 17.2% | −34% |
| **Cold Climate** | **Very Cold Winters** | **15.9%** | **3.1%** | **−80%** |
| | Dry Winters (*Dwd*) | 4.3% | 0.1% | −97% |
| | Dry Summers (*Dsd*) | 11.5% | 3.0% | −74% |
| | **Cold Summers** | **49.1%** | **43.8%** | **−11%** |
| | No Dry Season (*Dfc*) | 30.4% | 18.0% | −41% |
| | Dry Winters (*Dwc*) | 2.9% | 1.8% | −36% |
| | Dry Summers (*Dsc*) | 15.8% | 23.9% | 51% |
| | **Warm Summers** | **6.6%** | **18.7%** | **185%** |
| | No Dry Season (*Dfb*) | 4.3% | 12.9% | 197% |
| | Dry Winters (*Dwb*) | 0.2% | 1.2% | 518% |
| | Dry Summers (*Dsb*) | 2.1% | 4.6% | 126% |
| | **Hot Summers** | **2.0%** | **16.9%** | **733%** |
| | No Dry Season (*Dfa*) | 0.9% | 7.6% | 770% |
| | Dry Winters (*Dwa*) | 0.5% | 1.1% | 125% |
| | Dry Summers (*Dsa*) | 0.7% | 8.3% | 1099% |

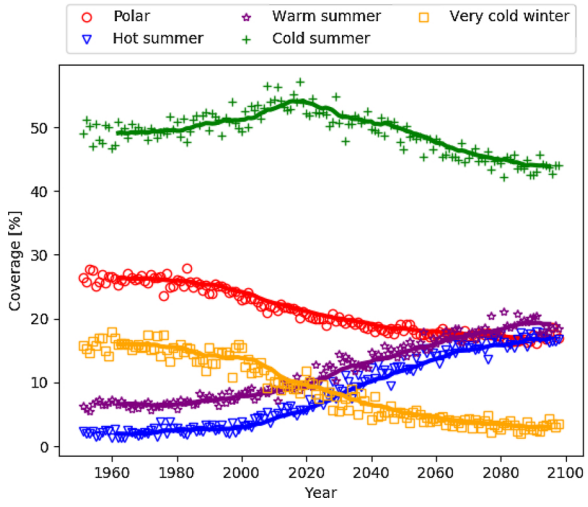


**Fig. 3.** Proportional coverage of the most common groups of KG classes in the Arctic, below 500 m.a.s.l. for the period 1951–2099. A 15-year rolling mean is shown as solid line.

exhibit this behavior in glaciated terrain. Hence, for further analysis of the results, Sen's method was used. The results in Fig. 4 show large areas of decreasing SCF at lower latitudes surrounding the Arctic circle, whereas at higher latitudes, around the shoreline of the Arctic seas patterns of increasing SCF were observed. Averaged across the arctic AMAP area below 500 m.a.s.l, the findings suggest a decrease in the SCF of 0.25%/year, or 9.1 days/decade, in the period 2001–2016.

### 3.3. Comparison of SCF and climate trends

We calculated the trends in annual coverage of the two most common KG classes and the average SCF trend in each of the ten study areas, as defined in Section 2.5. The trends were calculated for the overlapping period (2001–2016).

Fig. 5 shows the time series of proportional KG class coverage and SCF for this period. The results differed between areas with changes being evident in some places, whereas in other areas no clear changes were observed, neither for the snow nor the climate regimes. In general, warmer climate classes were observed to replace colder ones during the study period.

Furthermore, we assessed the evidence for the statistical significance of the KG trend line in each study area, using the methods described in Section 2.5. We also calculated the percentage of each area where a significant SCF trend was observed. Table 2 shows the changes in the two most common KG climate classes in all study areas and the result of the statistical analysis of whether the changes can be considered statistically significant. Table 2 also shows the portion of each area where a statistically significant SCF trend was observed, as described in Fig. 4. The table shows the total portion of significant SCF trends as well as the portions of positive and negative SCF trends. The results show that in seven study areas we identified a statistically significant trend in the coverage of one or both of the two main climate classes. These areas also had the biggest portion of statistically significant SCF trends (4.8–13.6% at $\alpha = 0.05$). In the three areas where the climate had not changed statistically significantly - Taymir Peninsula & the Norilsk area, Svalbard & Eastern Greenland area and the Canadian Arctic Archipelago – we also observed the smallest portion of significant SCF trends (< 2% at $\alpha = 0.05$). Hence, the results shown in Table 2 are consistent in that the most pronounced changes in snow cover were observed in areas where the most significant climate change had occurred.

Our results show that, across the AMAP area polar tundra (*ET*) has retreated significantly while at the same time SCF has decreased significantly in 2.8% of the area and increased in 0.8%, at the $\alpha = 0.05$ confidence level. Table 2 shows that in different study areas these trends vary considerably, although in all cases polar or cold summer climate classes are replaced by warmer climate classes.

In both the Lower Mackenzie river delta and the Northern Alaska & North slope area we observed climate with dry/hot summers (*Dsb*) advancing significantly while SCF has been increasing. In the Lena River Delta area cold summer regions with very cold winters (*Dfd*) have receded and cold/dry summer (*Dsc*) regions have advanced while SCF has increased. In the Chukotsky Peninsula, Polar Tundra (*ET*) has receded while SCF has increased. In these four areas we observed a pattern of warmer climate classes advancing at the same time as SCF is increasing. We suggest that the increased SCF observed are driven by changes in the precipitation regime, however, the KG classes that are changing in these areas do not lend themselves to detailed analysis of precipitation patterns.

In both the Kola Peninsula area and the Novaya Zemiya & Pechora Seas area, cold summer regions (*Dfc*) have receded and warm summer regions (*Dfb*) have advanced while SCF has decreased. On Baffin Island and in Western Greenland, polar tundra (*ET*) has receded and cold summer climate (*Dfc*) has advanced while SCF has increased and decreased by about the same amount.

## 4. Discussion

In this study we compared trends in climate change and snow cover frequency in the Arctic. Our results showed that KG climate classes associated with warm summers have been spreading northward in the Arctic, replacing cold summer climates and polar tundra. These changes are most evident at lower latitudes while colder climate classes are more persistent further north. This is consistent with the snow cover changes we observed at lower latitudes where we saw a decreasing SCF trend around the Arctic perimeter. These results also support our original hypothesis that warming climate would lead to decreasing

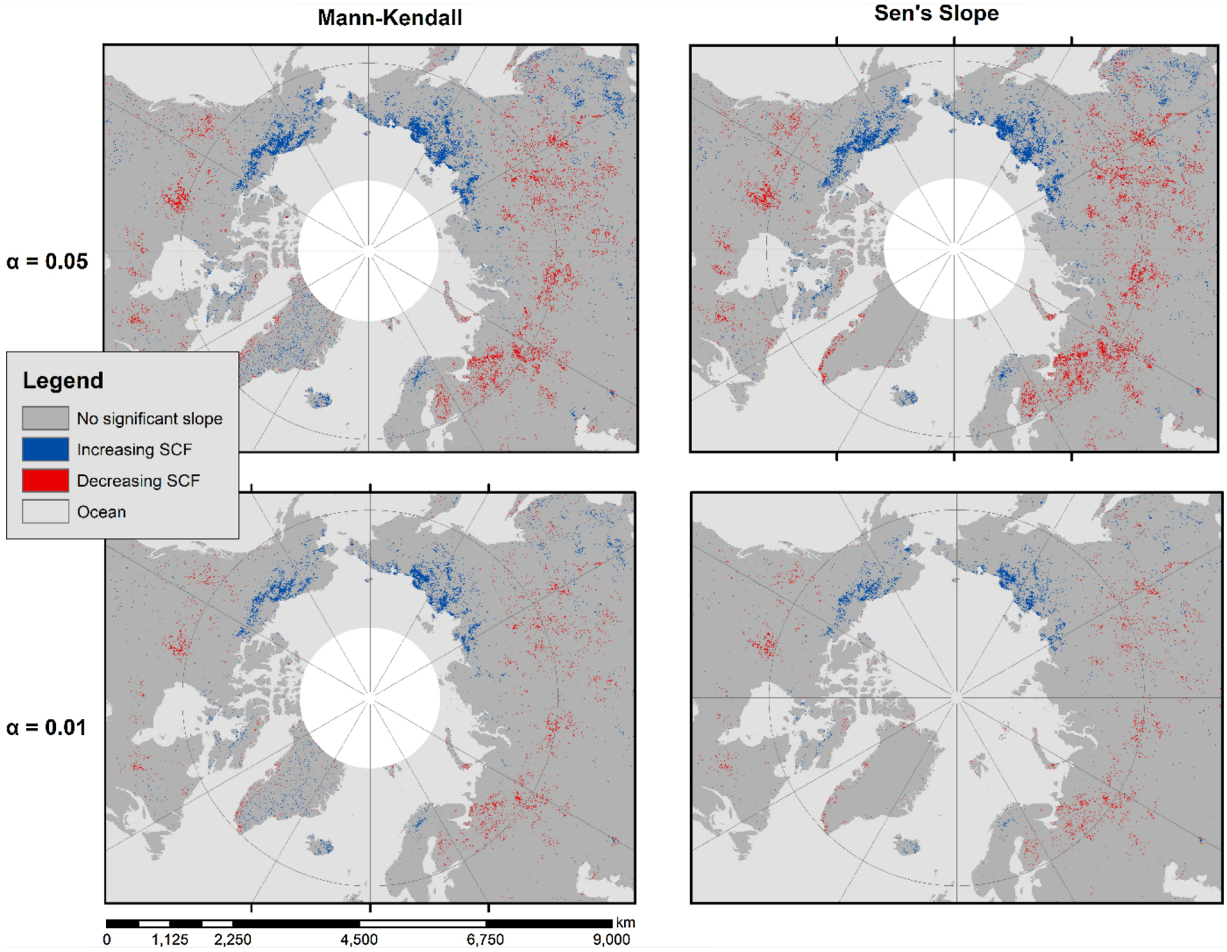


**Fig. 4.** Areas of significant slope in SCF, at significance levels α = 0.05 and α = 0.01 using the Mann Kendall hypothesis test (left) and Sen's slope estimator (right) (blue: increasing SCF, red: decreasing SCF) (For interpretation of the references to colour in this figure legend, the reader is referred to the web version of this article).

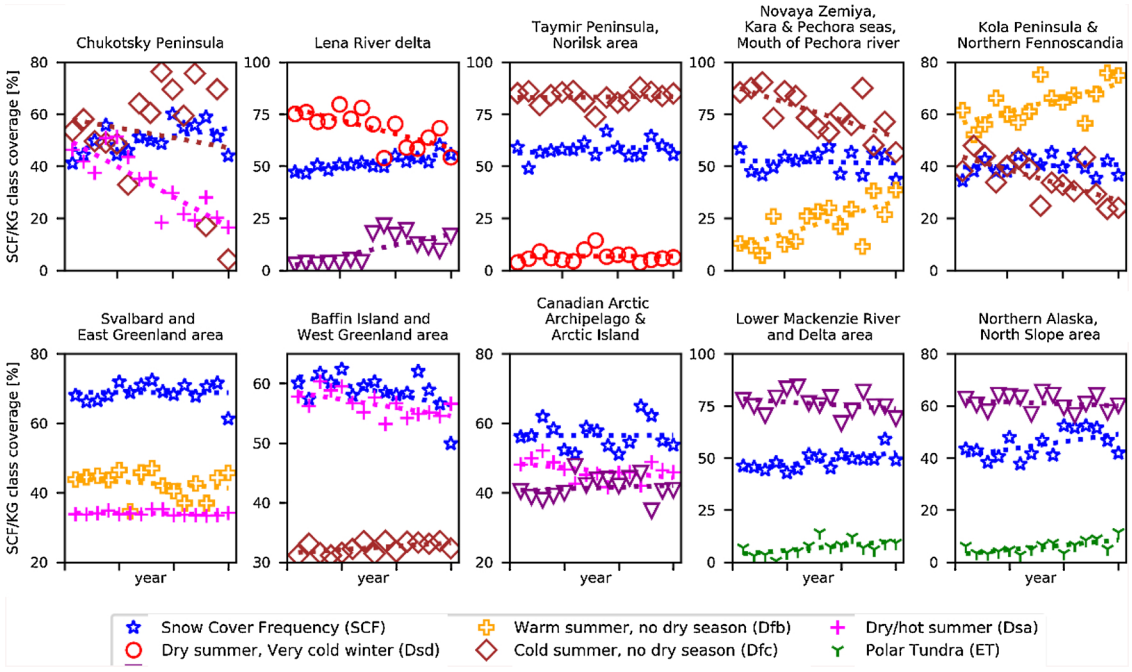
Chukotsky Peninsula
Lena River delta
Taymir Peninsula, Norilsk area
Novaya Zemiya, Kara & Pechora seas, Mouth of Pechora river
Kola Peninsula & Northern Fennoscandia
Svalbard and East Greenland area
Baffin Island and West Greenland area
Canadian Arctic Archipelago & Arctic Island
Lower Mackenzie River and Delta area
Northern Alaska, North Slope area
SCF/KG class coverage [%]
year
Snow Cover Frequency (SCF)
Dry summer, Very cold winter (Dsd)
Warm summer, no dry season (Dfb)
Cold summer, no dry season (Dfc)
Dry/hot summer (Dsa)
Polar Tundra (ET)

**Fig. 5.** SCF and proportional coverage of the two most common KG classes in each study area below 500 m.a.s.l. for the period 2001–2016. Trends were estimated with an ordinary least square linear regression (note, for clarity the subplots have differing scales on the vertical axis).

**Table 2**
Changes in coverage of the two main KG classes in the period 2001–2016 and the percentage of study areas below 500 m.a.s.l. showing a significant SCF trend. Significant results at the α = 0.05 confidence level are in bold.

| | 1st KG Class | | | | 2nd KG class | | | | SCF significant area [%] (%pos. / %neg.) | |
|---|---|---|---|---|---|---|---|---|---|---|
| Area | Name | Change 2001–2016 [%] | MK p-value | Sen's slope | Name | Change 2001–2016 [%] | MK p-value | Sen's slope | α = 0.05 | α = 0.01 |
| **Arctic AMAP area** | Cold summer no dry season (Dfc) | −7.7% | 0.255 | inSign | **Tundra (ET)** | **−5.99%** | **0.025** | **Sign** | 3.6 (+0.8/−2.8) | 0.9 (+0.2/−0.7) |
| **Chukotsky Peninsula** | Cold summer no dry season (Dfc) | −21.60% | 0.72 | inSign | **Tundra (ET)** | **−77.00%** | **0.0006** | **Sign** | 11.5 (+11.4/−0.07) | 3.7 (+3.7/−0.0) |
| **Lena River Delta** | **Cold summer very cold winter (Dfd)** | **−25.30%** | **0.006** | **Sign** | **Cold/dry summers (Dsc)** | **490.50%** | **0.005** | **Sign** | 13.6 (+12.9/−0.7) | 6.4 (+6.2/−0.2) |
| **Taymir Peninsula, Norilsk Area** | Cold summer no dry season (Dfc) | 0.70% | 0.881 | inSign | Dry summer very cold Winter (Dsd) | 13.30% | 0.805 | inSign | 1.8 (+1.4/−0.4) | 0.4 (+0.3/−0.1) |
| **Novaya Zemiya, Kara & Pechora Seas, Mouth of Pechora River** | **Cold summer no dry season (Dfc)** | **−30.20%** | **0.009** | **Sign** | **Warm summer no dry season (Dfb)** | **198.60%** | **0.006** | **Sign** | 4.8 (+0.5/−4.3) | 1.6 (+0.1/−1.5) |
| **Kola Peninsula & Northern Fennoscandia** | **Warm summer no dry season (Dfb)** | **29.60%** | **0.009** | **Sign** | **Cold summer no dry season (Dfc)** | **−62.20%** | **0.003** | **Sign** | 9.1 (+2.3/−6.8) | 3.6 (+0.7/−0.29) |
| **Svalbard and Eastern Greenland** | Warm summer no dry season (Dfb) | −3.40% | 0.52 | inSign | Tundra (ET) | −1.30% | 0.21 | inSign | 1.2 (+0.6/−1.6) | 0.9 (+0.2/−0.7) |
| **Baffin Island and West Greenland Area** | **Tundra (ET)** | **−7.00%** | **0.025** | **Sign** | **Cold summer no dry season (Dfc)** | **5.00%** | **0.042** | **Sign** | 7.8 (+3.1/−4.7) | 3.0 (+1.1/−1.9) |
| **Canadian Arctic Archipelago & Arctic Islands** | Tundra (ET) | −8.10% | 0.255 | inSign | Cold/dry summers (Dsc) | 6.50% | 0.22 | inSign | 1.3 (+0.08/−1.2) | 0.5 (+0.2/−0.3) |
| **Lower Mackenzie River and Delta area** | Cold/dry summers (Dsc) | −11.29% | 0.21 | inSign | **Dry/hot summers (Dsa)** | **32.78%** | **0.02** | **Sign** | 11.3 (+10.7/−0.6) | 4.5 (+4.3/−0.2) |
| **Northern Alaska and North slope area** | Cold/dry summers (Dsc) | 4.03% | 0.45 | inSign | **Dry/hot summers (Dsa)** | **84%** | **0.006** | **Sign** | 11.1 (+11.05/−0.05) | 4.3 (+4.3/−0.0) |

frequency of snow coverage. At high latitudes, however, around the Arctic shores, we observed increasing SCF trends in many areas, the opposite of our original hypothesis. This pattern was most obvious in areas close to the Bering Strait, and to a lesser extent in areas close to the Barents and Norwegian Seas.

We observed that 8.3% of the Arctic AMAP area has undergone a significant change in SCF in the MODIS period (2001–2016). Averaged across the Arctic SCF has decreased by 0.25%/year or by 9.1 days per decade. These findings agree with prior studies on changes to the snow regime in the area. Yunlong et al. (2018) used MODIS, AMSR-e and the IMS snow cover extent product to develop cloud-free daily snow cover extent maps and estimated a decrease in Northern Hemisphere (NH) Snow Covered Days (SCD) by 5.3 days/decade over the MODIS period; Hori et al. (2017) combined MODIS and AVHRR data to derive a daily Snow Cover Extent (SCE) product for the Northern Hemisphere and found a decreasing trend of 10 days/ decade over large areas of the NH during the period 1978–2015; Liston and Hiemstra (2011) modeled NH snow cover using MERRA reanalysis data and found a decrease in SCD by 2.5 days per decade across the Arctic in the period 1979 − 2009. On average these studies suggest that the frequency of snow cover in the Arctic has decreased by 6.7 days/decade.

In seven study areas of ten we observed evidence for statistically significant climate change during the period 2001–2016 These areas also showed the largest portions of statistically significant SCF trends. These areas have in common proximity to marine areas where sea ice concentration has decreased significantly in recent years (Maslanik et al., 2011). The three areas where no significant climate change and limited SCF trends were detected are all located in the far north and two are in or near the central continental Arctic where sea ice concentrations have not changed as dramatically. These results are consistent with previous findings that suggest that the decreasing sea ice concentrations in the surrounding seas have resulted in increased precipitation over these historically arid areas (Kopec et al., 2016). Although consistent with models (Singarayer et al., 2006) the increasing SCF trends we observed in this study are not found in the studies of Yunlong et al. (2018) or Hori et al. (2017).

In our study we used the MODIS TERRA snow cover product to quantify changes in snow cover. We did not use the MODIS AQUA products due to known issues with band 6 (Barnes et al., 2003). We calculated the SCF rather than performing gap filling and calculating the SCD to prevent adding uncertainty associated with the gap filling method. We suggest that further work should be done to validate and compare gap-filled and multi-sensor snow products to ground-based observations and modeling results to limit and quantify the uncertainty associated with these data. We note that the MODIS period, 2001–2016 is rather short, and trends during this short period can be induced by low frequency cyclical climate patterns, or by a small amount of extreme weather events. However, combined with the climate data we argue that trends observed in both the snow and climate regime during this period can be considered reliable. Both the KG climate classification and presence of snow cover are primarily dependent on precipitation and temperature. Although the mapping from the precipitation and temperature fields to the climate classification and SCF is quite different, our results show that statistically significant changes in these regimes are correlated and that snow cover trends are a useful indicator of assessing changes to regional climate.

Our analysis of climate classifications in the Arctic for the period 1951–2099 suggests that, according to the CMIP5 projections for rcp 4.5, the changes observed during the MODIS era are part of a larger trend that will continue throughout the present century. Given the consistency of the climate trends and their correlation to local snow cover changes, the SCF trends observed in the period 2001–2016 are unlikely to be an artifact of natural periodicity in the climate regime. We expect the northward progress of warmer climate classes will continue at least throughout the present century, as will the decreasing SCF trends as observed in this study. At the same time at higher latitudes, we expect SCF to continue increasing as sea ice concentration continues to decrease.

## 5. Conclusions

Across the Arctic we observed a consistent trend of warmer climate classes, associated with longer and warmer summers, spreading ever northward. In seven of ten study areas we observed evidence for significant climate change occurring in the period 2001–2016. In these same areas, we also observed the largest SCF trends. In general, we observed decreasing SCF trends at lower latitudes while further north, in the areas bordering the Arctic seas, we observed increasing SCF trends. This increase in SCF at high latitudes has most likely been from increased precipitation due to increasing humidity that results from a declining sea ice concentration. These results are consistent with prior studies in the area.

Our results show that, according to the CMIP5 projections for rcp 4.5, the climate changes observed in the Arctic since 2001 are part of a larger climatic trend that is expected to continue at least throughout the present century. Based on these projections we expect decreasing SCF trends to spread northward, while at higher latitudes, we expect SCF to continue increasing as sea ice concentrations decrease. These changes will impact the Arctic ecosystem, local communities and current exploitation of natural resources and potential utilization of new areas and resources, such as for mining, oil/gas extraction, and transportation.

## Conflicts of interest

The authors declare no conflict of interest. The funding sponsors had no role in the design of the study; in the collection, analyses, or interpretation of data; in the writing of the manuscript; nor in the decision to publish the results.

## Acknowledgments

We thank the University of Iceland Research Fund which is supporting the first author through the doctoral grants of the University of Iceland Research Fund and the Icelandic National Energy Company, Landsvirkjun, which supported the first author through the Energy Research Fund with grant no. DOK-02-2017. We also acknowledge the assistance of the facilitators at a workshop on scientific writing, arranged by Aalto University, Helsinki, Finland, and IWA/YWP Finland in August 2018.

## Appendix A. Köppen-Geiger Classification Criteria

See Table A1.

**Table A1**
Criteria for Köppen-Geiger classifications and their symbols.

| 1st | 2nd | 3rd | Description | Criteria* |
|---|---|---|---|---|
| A | | | Tropical | $T_{cold} \geq 18$ |
| | f | | -Rain forest | $P_{dry} \geq 60$ |
| | m | | -Monsoon | Not Af and $P_{dry} \geq 100\text{-}MAP/25$ |
| | w | | -Savannah | Not Af and $P_{dry} < 100\text{-}MAP/25$ |
| B | | | Arid | $MAP < 10*P_{threshold}$ |
| | w | | -Desert | $MAP < 5*P_{threshold}$ |
| | s | | -Steppe | $MAP \geq 5*P_{threshold}$ |
| | | H | -Hot | $MAT \geq 18$ |
| | | K | -Cold | $MAT < 18$ |
| C | | | Temperate | $T_{hot} > 10$ & $0 < T_{cold} < 18$ |
| | s | | -Dry Summer | $P_{sdry} < 40$ & $P_{sdry} < P_{wwet}/3$ |
| | w | | -Dry Winter | $P_{wdry} < P_{swet}/10$ |
| | f | | -Without dry season | Not Cs or Cw |
| | | A | -Hot Summer | $T_{hot} \geq 22$ |
| | | B | -Warm Summer | Not a & $T_{mon}10 \geq 4$ |
| | | C | -Cold Summer | Not a or b & $1 \leq T_{mon}10 \leq 4$ |
| D | | | Cold | $T_{hot} > 10$ and $T_{cold} \leq 0$ |
| | s | | -Dry Summer | $P_{sdry} < 40$ & $P_{sdry} < P_{wwet}/3$ |
| | w | | -Dry Winter | $P_{wdry} < P_{swet}/10$ |
| | f | | -Without dry season | Not Ds and Not Dw |
| | | A | -Hot Summer | $T_{hot} \geq 22$ |
| | | B | -Warm Summer | Not a & $T_{mon}10 \geq 4$ |
| | | C | -Cold Summer | Not a, b or d |
| | | D | -Very Cold Winter | Not a or b & $T_{cold} < -38$ |
| E | | | Polar | $T_{hot} < 10$ |
| | T | | -Tundra | $T_{hot} > 0$ |
| | F | | -Frost | $T_{hot} \leq 0$ |

## References


Ackerman, S.A., Holz, R.E., Frey, R., Eloranta, E.W., Maddux, B.C., McGill, M., 2008. Cloud detection with MODIS. Part II: validation. J. Atmos. Oceanic Technol. 25 (7), 1073–1086. https://doi.org/10.1175/2007JTECHA1053.1.

AMAP, 2015. AMAP Assessment 2015: Temporal Trends in Persistent Organic Pollutants in the Arctic. AMAP Assessment Report.

Ault, T.W., Czajkowski, K.P., Benko, T., Coss, J., Struble, J., Spongberg, A., et al., 2006. Validation of the MODIS snow product and cloud mask using student and NWS cooperative station observations in the Lower Great Lakes Region. Remote Sens. Environ. 105 (4), 341–353. https://doi.org/10.1016/j.rse.2006.07.004.

Baker, N., 2011. Joint Polar Satellite System (JPSS) VIIRS Snow Cover Algorithm Theoretical Basis Document (ATBD). Northrop Grumman Aerospace Syst., Redondo Beach, Calif, pp. 1–52.

Barichivich, J., Briffa, K.R., Myneni, R.B., Osborn, T.J., Melvin, T.M., Ciais, P., et al., 2013. Large-scale variations in the vegetation growing season and annual cycle of atmospheric CO2 at high northern latitudes from 1950 to 2011. Glob. Change Biol. 19 (10), 3167–3183. https://doi.org/10.1111/gcb.12283.

Barnes, W.L., Xiong, X., Salomonson, V.V., 2003. Status of Terra MODIS and Aqua MODIS. Adv. Space Res. 32 (11), 2099–2106. https://doi.org/10.1016/S0273-1177(03)90529-1.

Beck, C., Grieser, J., Rudolf, B., 2005. A New Monthly Precipitation Climatology for the Global Land Areas for the Period 1951 to 2000 Vol. 2004 Klimastatusbericht KSB.

Bokhorst, S., Pedersen, S.H., Brucker, L., Anisimov, O., Bjerke, J.W., Brown, R.D., et al., 2016. Changing Arctic snow cover: a review of recent developments and assessment of future needs for observations, modelling, and impacts. Ambio 45, 516. https://doi.org/10.1007/s13280-016-0770-0.

Chen, D., Chen, H.W., 2013. Using the Köppen classification to quantify climate variation and change: an example for 1901-2010. Environ. Dev. 6 (1), 69–79. https://doi.org/10.1016/j.envdev.2013.03.007.

Cohen, J., 1994. Snow cover and climate. Weather 49 (5), 150–156. https://doi.org/10.1002/j.1477-8696.1994.tb05997.x.

Cohen, J., Screen, J.A., Furtado, J.C., Barlow, M., Whittleston, D., Coumou, D., et al., 2014. Recent Arctic amplification and extreme mid-latitude weather. Nat. Geosci. 7, 627–637. https://doi.org/10.1038/ngeo2234.

Dietz, A.J., Kuenzer, C., Gessner, U., Dech, S., 2012. Remote sensing of snow – a review of available methods. Int. J. Remote Sens. 33 (13), 4094–4134. https://doi.org/10.1080/01431161.2011.640964.

Diffenbaugh, N.S., Scherer, M., Ashfaq, M., 2013. Response of snow-dependent hydrologic extremes to continued global warming. Nat. Clim. Change. https://doi.org/10.1038/nclimate1732.

Drapela, K., Drapelova, I., 2011. Application of Mann-Kendall test and the Sen's slope estimates for trend detection in deposition data from Bily Kriz (Beskydy Mts., the Czech Republic) 1997—2010. Beskydy 4 (2), 133–146. Retrieved from. http://www.mendelu.cz/dok_server/slozka.pl?id=57763%5Cndownload=88743.

Eliasson, K., Ulfarsson, G.F., Valsson, T., Gardarsson, S.M., 2017. Identification of development areas in a warming Arctic with respect to natural resources, transportation, protected areas, and geography. Futures 85, 14–29. https://doi.org/10.1016/j.futures.2016.11.005.

Frey, R.A., Ackerman, S.A., Liu, Y., Strabala, K.I., Zhang, H., Key, J.R., Wang, X., 2008. Cloud detection with MODIS. Part I: improvements in the MODIS cloud mask for Collection 5. J. Atmos. Oceanic Technol. 25 (7), 1057–1072. https://doi.org/10.1175/2008JTECHA1052.1.

Gocic, M., Trajkovic, S., 2013. Analysis of changes in meteorological variables using Mann-Kendall and Sen's slope estimator statistical tests in Serbia. Glob. Planet. Change 100, 172–182. https://doi.org/10.1016/j.gloplacha.2012.10.014.

Gorelick, N., Hancher, M., Dixon, M., Ilyushchenko, S., Thau, D., Moore, R., 2016. Google Earth Engine: planetary-scale geospatial analysis for everyone. Remote Sens. Environ. 202, 18–27. https://doi.org/10.1016/j.rse.2017.06.031.

Guan, B., Molotch, N.P., Waliser, D.E., Jepsen, S.M., Painter, T.H., Dozier, J., 2013. Snow water equivalent in the Sierra Nevada: blending snow sensor observations with snowmelt model simulations. Water Resour. Res. 49 (8), 5029–5046. https://doi.org/10.1002/wrcr.20387.

Hall, D.K., Riggs, G.A., Salomonson, V.V., 2006. MODIS/Terra Snow Cover Daily L3 Global 500m Grid V005 2000-01-01 to 2016-12-31. Retrieved January 5, 2017, from. https://nsidc.org/data/mod10a1.

Helsel, D.R., Hirsch, R.M., 2002. Statistical methods in water resources. Techniques of Water-Resources Investigations of the United States Geological Survey Vol. 36. pp. 524. https://doi.org/10.2307/1269385.

Hori, M., Sugiura, K., Kobayashi, K., Aoki, T., Tanikawa, T., Kuchiki, K., et al., 2017. A 38-year (1978–2015) Northern Hemisphere daily snow cover extent product derived using consistent objective criteria from satellite-borne optical sensors. Remote Sens. Environ. 191, 402–418. https://doi.org/10.1016/j.rse.2017.01.023.

Huang, C., Newman, A.J., Clark, M.P., Wood, A.W., Zheng, X., 2017. Evaluation of snow data assimilation using the ensemble Kalman filter for seasonal streamflow prediction in the western United States. Hydrol. Earth Syst. Sci. https://doi.org/10.5194/hess-21-635-2017.

Kopec, B.G., Feng, X., Michel, F.A., Posmentier, E.S., 2016. Influence of sea ice on Arctic precipitation. Proc. Natl. Acad. Sci. 113 (1), 46–51. https://doi.org/10.1073/pnas.1504633113.

Köppen, W., 1918. Klassifikation der Klimate nach Temperatur, Niederschlag und Jahresablauf (Classification of climates according to temperature, precipitation and seasonal cycle). Petermanns Geographische Mitteilungen.

Kottek, M., Grieser, J., Beck, C., Rudolf, B., Rubel, F., 2006. World map of the Köppen-Geiger climate classification updated. Meteorol. Z. 15 (3), 259–263. https://doi.org/10.1127/0941-2948/2006/0130.

Larsen, J.N., Anisimov, O.A., Constable, A., Hollowed, A.B., Maynard, N., Prestrud, P., et al., 2015. Polar regions. Climate Change 2014: Impacts, Adaptation and Vulnerability: Part B: Regional Aspects: Working Group II Contribution to the Fifth Assessment Report of the Intergovernmental Panel on Climate Change. https://doi.org/10.1017/CBO9781107415386.008.

Lawrence, D.M., Slater, A.G., Tomas, R.A., Holland, M.M., Deser, C., 2008. Accelerated Arctic land warming and permafrost degradation during rapid sea ice loss. Geophys. Res. Lett. 35, L11506. https://doi.org/10.1029/2008GL033985.

Liston, G.E., Hiemstra, C.A., 2011. The changing cryosphere: Pan-Arctic snow trends (1979–2009). J. Clim. 24 (21), 5691–5712. https://doi.org/10.1175/JCLI-D-11-00081.1.

Liu, Y., Key, J.R., Frey, R.A., Ackerman, S.A., Menzel, W.P., 2004. Nighttime polar cloud detection with MODIS. Remote Sens. Environ. 92 (2), 181–194. https://doi.org/10.1016/j.rse.2004.06.004.

Lohmann, U., Sausen, R., Bengtsson, L., Cubasch, U., Perlwitz, J., Roeckner, E., 1993. The Koppen climate classification as a diagnostic tool for general circulation models. Clim. Res. 3 (3), 177–193. https://doi.org/10.3354/cr003177.

LP-DAAC, 2004. Global 30 Arc-Second Elevation Data Set GTOPO30.

Maslanik, J., Stroeve, J., Fowler, C., Emery, W., 2011. Distribution and trends in Arctic sea ice age through spring 2011. Geophys. Res. Lett. 38, L13502. https://doi.org/10.1029/2011GL047735.

Maurer, E.P., Rhoads, J.D., Dubayah, R.O., Lettenmaier, D.P., 2003. Evaluation of the snow-covered area data product from MODIS. Hydrol. Process. 17 (1), 59–71. https://doi.org/10.1002/hyp.1193.

Maurice, G., Kendall, 1975. Rank Correlation Methods. Griffin, London.

Notz, D., Stroeve, J., 2016. Observed Arctic sea-ice loss directly follows anthropogenic CO2 emission. Science 354, 747–750. https://doi.org/10.1126/science.aag2345.

Oliphant, T.E., 2007. Python for scientific computing. Comput. Sci. Eng. 9 (3), 10–20. https://doi.org/10.1109/MCSE.2007.58.

Overland, J.E., Wang, M., Walsh, J.E., Stroeve, J.C., 2013. Future Arctic climate changes: adaptation and mitigation time scales. Earth's Future 2, 68–74. https://doi.org/10.1002/2013EF000162.Received.

Peel, M.C., Finlayson, B.L., Mcmahon, T.A., 2007. Updated world map of the Koppen-Geiger climate classification. HESSD Earth Syst. Sci. Discuss 4 (4), 439–473. https://doi.org/10.1127/0941-2948/2006/0130.

Sen, P.K., 1968. Estimates of the regression coefficient based on Kendall's Tau. J. Am. Stat. Assoc. 63 (324), 1379–1389. https://doi.org/10.1080/01621459.1968.10480934.

Singarayer, J.S., Bamber, J.L., Valdes, P.J., Singarayer, J.S., Bamber, J.L., Valdes, P.J., 2006. Twenty-first-century climate impacts from a declining Arctic sea ice cover. J. Clim. 19 (7), 1109–1125. https://doi.org/10.1175/JCLI3649.1.

Souri, A.H., Azizi, A., 2013. Removing bowtie phenomenon by correction of panoramic effect in MODIS imagery. Int. J. Comput. Appl. 68, 12–16 Published by Foundation of Computer Science, New York, USA.

Spinoni, J., Vogt, J., Naumann, G., Carrao, H., Barbosa, P., 2015. Towards identifying areas at climatological risk of desertification using the Köppen-Geiger classification and FAO aridity index. Int. J. Climatol. 35 (9), 2210–2222. https://doi.org/10.1002/joc.4124.

Stocker, T.F., Qin, D., Plattner, G.K., Tignor, M.M.B., Allen, S.K., Boschung, J., et al., 2013. Climate change 2013 the physical science basis: Working Group I contribution to the fifth assessment report of the intergovernmental panel on climate change. Climate Change 2013 the Physical Science Basis: Working Group I Contribution to the Fifth Assessment Report of the Intergovernmental Panel on Climate Change. https://doi.org/10.1017/CBO9781107415324.

Taylor, K.E., Stouffer, R.J., Meehl, G.A., 2012. An overview of CMIP5 and the experiment design. Bull. Am. Meteorol. Soc. 93, 485–498. https://doi.org/10.1175/BAMS-D-11-00094.1.

Thrasher, B., Melton, F., Weile, W., 2006. NASA Earth Exchange Global Daily Downscaled Projections (NEX-GDDP) | CDS. Retrieved May 1, 2017, from. https://cds.nccs.nasa.gov/nex-gddp/.

Thuiller, W., Albert, C., Araújo, M.B., Berry, P.M., Cabeza, M., Guisan, A., et al., 2008. Predicting global change impacts on plant species' distributions: future challenges. Perspect. Plant Ecol. Evol. Syst. https://doi.org/10.1016/j.ppees.2007.09.004.

van Vuuren, D.P., Edmonds, J., Kainuma, M., Riahi, K., Thomson, A., Hibbard, K., et al., 2011. The representative concentration pathways: an overview. Clim. Change 109 (1), 5–31. https://doi.org/10.1007/s10584-011-0148-z.

Wang, T., Fetzer, E.J., Wong, S., Kahn, B.H., Yue, Q., 2016. Validation of MODIS cloud mask and multilayer flag using CloudSat-CALIPSO cloud profiles and a cross-reference of their cloud classifications. J. Geophys. Res. 121 (19), 11620–11635. https://doi.org/10.1002/2016JD025239.

Wasserstein, R.L., Lazar, N.A., 2016. The ASA's statement on p-values: context, process, and purpose. Am. Stat. 70 (2), 129–133. https://doi.org/10.1080/00031305.2016.1154108.

Xu, W., Ma, H., Wu, D., Yuan, W., 2017. Assessment of the daily cloud-free MODIS Snow-cover product for monitoring the snow-cover phenology over the Qinghai-Tibetan Plateau. Remote Sens. 9 (6). https://doi.org/10.3390/rs9060585.

Yunlong, W., Huang, X., Hui, L., Sun, Y., Qisheng, F., Tiangang, L., 2018. Tracking snow variations in the Northern Hemisphere using multi-source remote sensing data (2000–2015). Remote Sens. 10 (1), 136. https://doi.org/10.3390/rs10010136.